Title
HIGH-RESOLUTION IMAGING OF PHIBSS z ~ 2 MAIN-SEQUENCE GALAXIES IN CO J = 1 → 0

Journal
The Astrophysical Journal, 809(2)

ISSN
0004-637X

Authors
Bolatto, AD
Warren, SR
Leroy, AK
et al.

Publication Date
2015-08-20

DOI
10.1088/0004-637x/809/2/175

Draft version October 10, 2018
Preprint typeset using LaTeX style emulateapj v. 01/23/15

HIGH RESOLUTION IMAGING OF PHIBSS $Z \sim 2$ MAIN SEQUENCE GALAXIES IN CO $J = 1 \rightarrow 0$

A. D. Bolatto[1], S. R. Warren[1], A. K. Leroy[2], L. J. Tacconi[3], N. Bouché[4,16], N. M. Förster Schreiber[3], R. Genzel[3,14,15], M. C. Cooper[5], D. B. Fisher[6], F. Combes[7], S. García-Burillo[8], A. Burkert[3,9], F. Bournaud[10], A. Weiss[11], A. Saintonge[12], S. Wuyts[3], & A. Sternberg[13]

Draft version October 10, 2018

ABSTRACT

We present Karl G. Jansky Very Large Array observations of the CO $J = 1 - 0$ transition in a sample of four $z \sim 2$ main sequence galaxies. These galaxies are in the blue sequence of star-forming galaxies at their redshift, and are part of the IRAM Plateau de Bure HIgh-z Blue Sequence Survey (PHIBSS) which imaged them in CO $J = 3 - 2$. Two galaxies are imaged here at high signal-to-noise, allowing determinations of their disk sizes, line profiles, molecular surface densities, and excitation. Using these and published measurements, we show that the CO and optical disks have similar sizes in main-sequence galaxies, and in the galaxy where we can compare CO $J = 1 - 0$ and $J = 3 - 2$ sizes we find these are also very similar. Assuming a Galactic CO-to-H_2 conversion, we measure surface densities of $\Sigma_{\rm mol} \sim 1200$ M$_\odot$ pc^{-2} in projection and estimate $\Sigma_{\rm mol} \sim 500 - 900$ M$_\odot$ pc^{-2} deprojected. Finally, our data yields velocity-integrated Rayleigh-Jeans brightness temperature line ratios r_{31} that are approximately unity. In addition to the similar disk sizes, the very similar line profiles in $J = 1 - 0$ and $J = 3 - 2$ indicate that both transitions sample the same kinematics, implying that their emission is coextensive. We conclude that in these two main sequence galaxies there is no evidence for significant excitation gradients or a large molecular reservoir that is diffuse or cold and not involved in active star-formation. We suggest that r_{31} in very actively star-forming galaxies is likely an indicator of how well mixed the star formation activity and the molecular reservoir are.

Keywords: galaxies: evolution, galaxies: ISM, galaxies: high-redshift, ISM: molecules

1. INTRODUCTION

Galaxy formation and evolution are regulated by the interplay between the hierarchical merging of dark matter halos, the accretion of primordial and recycled gas, the transport of gas within galaxy disks, and the subsequent gravitational fragmentation, phase transition, and formation of molecular clouds. The star formation that is the end-point of this process gives rise to nucleosynthesis, and metal-enriched outflows driven by stellar winds, radiation pressure, supernovae, and AGN activity (e.g., Davé et al. 2011a,b). These mechanisms interact in complex ways, giving rise to the rich phenomenology observed in galaxies today.

Surveys at $z \sim 1 - 2$ have shown that most star-forming galaxies (SFGs) populate a tight main sequence (Noeske et al. 2007; Daddi et al. 2007; Rodighiero et al. 2010), suggesting that the evolution of a typical galaxy is regulated by secular processes related to gas accretion from the cosmic web, with subsequent star formation, galactic outflows, and reaccretion of gas (e.g., Oppenheimer et al. 2010; Bouché et al. 2010; Davé et al. 2012; Lilly et al. 2013; Forbes et al. 2014). The gas accretion is provided by a combination of smooth and lumped accretion, the latter likely in the form of minor mergers (e.g., Kereš et al. 2005; Dekel et al. 2009b; Brooks et al. 2009). In this paradigm major mergers play a secondary role at forming the majority of galaxies, but are still critical for creating the most massive and the most actively star-forming galaxies. Until recently, almost all of the observations of gas in galaxies at high redshift targeted the rare "behemoths" (see Carilli & Walter 2013), typically quasar hosts or merging galaxies bright at submillimeter wavelengths (or even merging groups of galaxies, Ivison et al. 2013). The exceptions were a few intrinsically faint but highly lensed objects, where lensing complicates the data interpretation (Baker et al. 2004; Coppin et al. 2007; Riechers et al. 2010). The increased sensitivity in the millimeter-wave regime makes it now possible to directly observe normal massive star-forming

bolatto@astro.umd.edu
[1] Department of Astronomy and Joint Space Institute, University of Maryland, College Park, MD 20642, USA
[2] Department of Astronomy, Ohio State University, Columbus, OH 43210, USA
[3] Max-Planck-Institut für Extraterrestrische Physik (MPE), Giessenbachstr., D-85748 Garching, Germany
[4] CNRS/IRAP, 14 Avenue E. Belin, F-31400 Toulouse, France
[5] Department of Physics & Astronomy, Frederick Reines Hall, University of California, Irvine, CA 92697
[6] Centre for Astrophysics and Supercomputing, Swinburne University of Technology, P.O. Box 218, Hawthorn, VIC 3122, Australia
[7] Observatoire de Paris, LERMA, CNRS, 61 Av. de l'Observatoire, F-75014 Paris, France
[8] Observatorio Astronómico Nacional-OAN, Observatorio de Madrid, Alfonso XII, 3, 28014 - Madrid, Spain
[9] Universitätssternwarte der Ludwig-Maximiliansuniversität , Scheinerstr. 1, D-81679 München, Germany
[10] Service d'Astrophysique, DAPNIA, CEA/Saclay, F-91191 Gif-sur-Yvette Cedex, France
[11] Max Planck Institut für Radioastronomie (MPIfR), Auf dem Hügel 69, 53121 Bonn, Germany
[12] Department of Physics & Astronomy, University College London, Gower Place, London WC1E 6BT, UK
[13] School of Physics and Astronomy, Tel Aviv University, Tel Aviv 69978, Israel
[14] Department of Physics, Le Conte Hall, University of California, Berkeley, CA 94720, USA
[15] Department of Astronomy, Campbell Hall, University of California, Berkeley, CA 94720, USA
[16] University Paul Sabatier of Toulouse/ UPS-OMP/ IRAP, F-31400 Toulouse, France

galaxies at high redshift. Indeed, high-z main sequence SFGs are considerably more active in star formation than similar mass galaxies at $z = 0$, likely because they are richer in gas than present day blue sequence galaxies, as found by molecular gas observations (Tacconi et al. 2010, 2013; Daddi et al. 2010a,b).

Early universe molecular gas surveys usually target the mid-J transitions of the CO molecule, which are accessible for $1 < z < 3$ in the transparent 1−3 mm atmospheric windows. Additionally, for a fixed gas mass and typical conditions these transitions are more luminous and easier to detect than the ground level transition. This, however, introduces an additional source of uncertainty when converting their fluxes to H_2 masses at high-z (Weiss et al. 2007; Carilli & Walter 2013). Excitation data remain scarce for high-z SFGs. The lowest galaxy luminosities currently probed by high redshift CO observations correspond to the high luminosity end of the main sequence, and the data suggest their excitation is intermediate between that observed in high-z Submillimeter Galaxies (SMGs) or local Ultra-Luminous IR Galaxies (ULIRGs), and the Milky Way (Fixsen et al. 1999). Observations find CO main-beam velocity-integrated Rayleigh-Jeans brightness temperature line ratios $r_{31} \equiv T_{mb}\Delta v(J = 3-2)/T_{mb}\Delta v(J = 1-0) \sim 0.3-0.8$ in a handful of high-z main sequence SFGs (Dannerbauer et al. 2009; Aravena et al. 2010; Riechers et al. 2010; Aravena et al. 2014). The excitation picture, however, is not clear cut. Studies of samples of local and high-z luminous and ultraluminous IR galaxies also suggests a typical $r_{31} \sim 0.6$ with very large dispersions (Harris et al. 2010; Papadopoulos et al. 2011; Ivison et al. 2011; Greve et al. 2014).

The observed r_{31} in high-z main sequence SFGs can be reproduced by a range of conditions. The typical conditions found in the highly idealized single-component models are $T_{kin} \approx 90$ K with $n \approx 600$ cm^{-3} to $T_{kin} \approx 10$ K with $n \approx 2500$ cm^{-3}, together with gas filling factors from 2% to 8% (Aravena et al. 2010). This interpretation is by no means unique, however, as realistic galaxies contain multiple components, and different transitions may not be necessarily coextensive — for example if dense warm star-forming regions were surrounded by cooler, less dense envelopes of gas (e.g. Harris et al. 2010). It is also possible to hide a significant amount of mass in a cold component that would be hard to detect (Papadopoulos et al. 2012). The inclusion of $J > 3$ transitions reveals that, at least in some of the main sequence SFGs, the "one component" picture of the ISM is too simplistic, although the data support the idea of a somewhat lower excitation in main sequence galaxies than in SMGs (Daddi et al. 2014; Bournaud et al. 2014a). In particular, the T_{kin} and n inferred above would produce too little, if any, $J > 4$ emission in contrast with the observations. Better sensitivity observations of the $J = 1-0$ transition, observations of transitions with $J > 3$, and higher spatial resolutions are necessary to definitively constrain the molecular excitation in these galaxies.

There are a handful of resolved molecular measurements of $z \sim 1-2$ main sequence galaxies. Tacconi et al. (2010) discusses in particular $J = 3-2$ observations of one $z \sim 1.5$ SFG at a resolution of $\theta \sim 0\farcs65$ that reveal a collection of clumps with gas masses of $\sim 5 \times 10^9$ M$_\odot$, sizes of $\sim 2-4$ kpc, and surface densities ≥ 500 M$_\odot$ pc^{-2}. Tacconi et al. (2013) expands on these results, determining ~ 20 CO $J = 3-2$ sizes (mostly for $z \sim 1$ objects), reaching the conclusion that the UV/optical disk size and the CO size are similar. Genzel et al. (2013) examine high-resolution observations of the $z \sim 1.5$ galaxy EGS13011166, a disky system with massive clumps and a globally unstable gas disk. Freundlich et al. (2013) take advantage of position-velocity information to apportion the $J = 3-2$ emission from four $z \sim 1.5$ SFGs in clumps, inferring typical gas surface densities $\Sigma_{\rm mol} \sim 400$ M$_\odot$ pc^{-2} with a large dispersion. Aravena et al. (2014) presents a few $J = 1-0$ observations of $z \sim 1-2$ SFGs, including an earlier dataset for the $z = 2.2$ galaxy BX610, one of the sources studied in this paper. In the $z \sim 1.5$ SFG that they observe at high resolution they find clumps with masses $\sim 4-9 \times 10^9$ M$_\odot$ that make up 40% of the emission. Giant clumps are a natural consequence of the gas richness of these high-z systems, which makes their disks unstable (e.g., Dekel et al. 2009a; Genzel et al. 2013; Bournaud et al. 2014b). A clumpy morphology has also been observed in the relatively rare, very gas-rich and strongly star-forming local disks (Green et al. 2014; Fisher et al. 2014).

In this work we present new, very sensitive observations of the CO $J = 1-0$ transition in main sequence SFGs at redshift $z \sim 2.3$, during the peak of cosmic star formation. We discuss the observations and data reduction in §2. In §3 we present and discuss the results; particularly focusing on sizes, surface densities, and excitation. In §4 we summarize them and present the conclusions.

2. OBSERVATIONS AND REDUCTION

We selected our sources as the brightest CO $J = 3-2$ emitters at $z \sim 2.2-2.3$ in the IRAM Plateau de Bure HIgh-z Blue Sequence Survey (PHIBSS) sample (Tacconi et al. 2010, 2013). Original optical data for these objects are discussed by Erb et al. (2006). We observed the CO (J=1−0) transition at 115.2712 GHz rest frequency in Q1700MD94, Q2343BX610, Q1700MD69, and Q1700MD174 using the Karl G. Jansky Very Large Array (Jansky VLA) in the C- and D-array configurations, with typical angular resolution of $\sim 0.7''$ and $\sim 2''$ respectively. In order to observe the redshifted CO line the observations employ the Ka-band receiver, which covers the frequency range $26.5-40.0$ GHz.

C-array observations were carried out between 12 October 2010 and 09 January 2011 under project 10B-106. These data were obtained during the VLA to Jansky VLA upgrade transition period, resulting in a reduced bandwidth. Each C-array observation has 0.5 MHz spectral resolution and covers a 128 MHz bandwidth centered on the redshifted frequencies of our galaxies (34.55 GHz, 35.90 GHz, 35.06 GHz, and 34.49 GHz for MD94, BX610, MD69, and MD174 respectively).

The follow up D-array data were taken between 07 February 2013 and 07 April 2013 under project 13A-115. These data have 1 MHz spectral resolution with a total of 4 GHz bandwidth coverage. The time invested is approximately 8 hours per source in C-array. The D-array follow up spent 4.5 hours on MD94 and 8.5 hours on BX610. Because only ~ 40% of the visibilities in C-array have uv distances $\leq 10^5$ kλ (probing size scales $\gtrsim 2''$),

and the sources were found to be extended in the original observations, the sensitivity added by the D-array observations is very significant.

All data were processed using the Jansky VLA reduction pipeline[17] version 1.2.0 using the Common Astronomy Software Applications package (CASA) version 4.1. The fluxes employed for the flux calibrators were applied in the pipeline following the prescribed fits by Perley & Butler (2013). We visually inspected each observation after the calibration scripts were completed to flag a few remaining bad baselines. The source was then split off from each individual observation and combined into a single data set for imaging. After imaging with 50 km s^{-1} channel widths, we cleaned down to $\sim 1\sigma$ on a $5''\times5''$ box centered on the source. The image cubes span a range of ±1000 km s^{-1} around the optical redshift of the source for MD94 ($z = 2.336$) and BX610 ($z = 2.211$), while MD69 ($z = 2.288$) and MD174 ($z = 2.342$) were imaged over a ±500 km s^{-1} span because of the reduced bandwidth available in the transition period during which the C-array data were acquired. For the calculation of physical parameters we use a standard cosmology ($H_0 = 69.6$ km s^{-1} Mpc^{-1}, $\Omega_M = 0.315$, $\Omega_\Lambda = 0.685$, Komatsu et al. 2014).

BX610: One C-array track was not included in the imaging because of strong pattern noise (maybe due to interference or correlator problems), but this problem persists at a lower level in the remainder of the C-array data for this object. The flux and gain calibrators for BX610 were 3C48 and J2346+0930, respectively. At our observing frequency 3C48 has a flux density of $S_\nu = 802$ mJy which was applied to our data to fix the flux scale. The resulting flux of the gain calibrator was 470 mJy in the C-array data and 325 mJy in the D-array data. We inserted a second calibrator in the D-array observations (J2330+110) to check the quality of the calibration including phase transfer. The recovered flux of the check calibrator is 660 mJy, in excellent agreement with the power-law interpolation between the 2 cm and 0.7 cm fluxes listed in the VLA calibrator catalog for this object of 640 mJy. The synthesized beam sizes range from $0\farcs83 \times 0\farcs63$ (C only, natural weighting) to $1\farcs44 \times 1\farcs21$ (C+D, Briggs weighting with robust parameter set to 0.5, henceforth "robust weighting") and $2\farcs02 \times 1\farcs87$ (C+D, natural weighting). The 1σ noise per 50 km s^{-1} channel for the robust C+D cube is 52 μJy beam^{-1}. The high resolution $J = 3 - 2$ data were obtained at PdBI as part of PHIBSS, and have a resolution $1\farcs5 \times 0\farcs7$.

MD94: Along with MD94, flux (3C286) and gain (J1645+6330) calibrators were also observed. 3C286 has a flux density of ≈1800 mJy at 34.55 GHz which was used to fix the flux scale of the data. The derived flux density of our gain calibrator was 370 mJy in the C-array data and 500 mJy in the D-array data. We also included a secondary calibrator in the observations (J1716+6836). Applying the gain solution to this object recovers $S_\nu \approx 430$ mJy while the VLA calibrator catalog would lead us to expect ~ 670 mJy. However, given its listed fluxes this calibrator appears to be a highly variable flat spectrum source, and it is very likely that changes are due to intrinsic variability. The synthesized beam sizes range from $0\farcs77 \times 0\farcs72$ (C only, natural weighting) to $0\farcs95 \times 0\farcs89$ (C+D, robust weighting) and $1\farcs70 \times 1\farcs55$ (C+D, natural weighting). The 1σ noise per channel for the robust C+D cube is 58 μJy beam^{-1}.

MD174 & MD69: These sources were not clearly detected in C-array observations and were not followed with D-array. Both galaxies were flux calibrated with observations of 3C286 and antenna gains were corrected with observations of J1645+6330. The resulting rms noise per 50 km s^{-1} channel is approximately 78 and 68 μJy beam^{-1} for MD174 and MD69, respectively. The integrated intensity maps of both objects show positive signal at the position of the source that, while formally close to 3σ for MD69, is hard to distinguish from many nearby noise peaks. The smoothed spectrum at the position of MD69 shows what may be a marginally significant line. The $J = 1 - 0$ luminosities of these objects in Table 1 can be compared to their respective $J = 3 - 2$ luminosities of 1.9 and 1.1×10^{10} K km s^{-1} pc^2 (Tacconi et al. 2013). The resulting ratios are consistent with our conclusions for MD94 and BX610 in §3.3, but do not add significant information.

3. RESULTS AND DISCUSSION

Both MD94 and BX610 are detected at good signal-to-noise, even in the C-only data (Figure 1). MD69 and MD174, which are weaker sources in the CO $3 - 2$ observations, were not clearly detected and not followed up with D array observations, therefore we focus our discussion on the previous two galaxies. Together with the earlier publication of another BX610 dataset (Aravena et al. 2014), these constitute the first CO $J = 1 - 0$ detections of unlensed $z > 1.5$ main sequence galaxies, and the first observations where measurements of the intrinsic properties of the cold CO disks of main sequence galaxies free of lensing corrections are possible at these redshifts.

Employing the parametrization of the main sequence of star-forming galaxies derived for the AEGIS and COSMOS fields by Whitaker et al. (2012), both MD94 and BX610 are very representative of the massive end of the main sequence at their $z \sim 2.3$ redshift. Their specific star formation rates are sSFR$\sim 1.8\times10^{-9}$ and 2.1×10^{-9} yr^{-1} respectively, which at their inferred stellar masses ($M_* \approx 1.5\times10^{11}$ and 1.0×10^{11} $M_\odot$ respectively) places them well within the main sequence 0.3 dex scatter. Both are very active star-forming galaxies, with respective SFR$\sim 271\pm95$ and 212 ± 74 $M_\odot$ yr^{-1} (Tacconi et al. 2013). MD94, the most massive of the pair, displays a broad Hα line and is classified as an AGN (Erb et al. 2006). BX610 may contain an AGN, but not a very luminous one (Förster Schreiber et al. 2014; Newman et al. 2014; Genzel et al. 2014). It is important to keep in mind that these galaxies were selected because they are bright CO $J = 3 - 2$ emitters, which makes it possible to target them in CO $J = 1 - 0$, and thus their CO properties may not be representative of the population as a whole. Our CO measurements are summarized in Table 1, and the resulting physical parameters in Table 2 together with relevant parameters from Tacconi et al. (2013).

3.1. *The Size of the Molecular Disks in High-z Main Sequence Galaxies*

[17] The Jansky VLA reduction pipeline is available for download at this url: https://science.nrao.edu/facilities/vla/data-processing/pipeline

MD94 is clearly resolved in the observations (c.f., Table 1). The simple Gaussian fit (CASA `imfit`) yields an elongated source in the N-S direction, with deconvolved FWHM diameter (after averaging the C-only and C+D robust results) of $\sim 1\farcs3 \times 1\farcs0$ at high significance ($\geq 5\sigma$). With an image scale of ~ 8.4 kpc per arcsecond at this redshift, this corresponds to $\sim 11 \times 8$ kpc. The residual RMS in the central region after removing the Gaussian fit is very similar to that measured in empty regions of the original image, showing that a 2D Gaussian is a good model for the source at this signal-to-noise. BX610 is clearly resolved along its major axis, with a deconvolved CO FWHM diameter of $1\farcs6 \times 0\farcs6$ corresponding to $\sim 13 \times 5$ kpc (for this source we adopt the results of the C+D robust combination, which despite the larger beam is better behaved than the C-only observation). We also did UV-plane model fitting using the `uvmodelfit` task in CASA, and the results are essentially identical to those from image-plane fitting.

In $z = 0$ galaxies there is a good relation between the sizes of molecular and stellar disks (e.g., Regan et al. 2001). The CO emission is found in an approximately exponential disk with a $R_{\rm CO}$ scale-length that is $R_{\rm CO} \simeq 0.2\,R_{25}$, the isophotal radius of the B-band light at 25^{th} magnitude (Young & Scoville 1991; Young et al. 1995; Schruba et al. 2011). Consequently half of the CO emission in local disks is contained within a radius $R_{1/2,\rm CO} = 0.34\,R_{25}$. For optical light it is usually assumed that the stellar disk scale length is $R_* \sim 0.25\,R_{25}$ (implying an effective radius containing half the optical light of $R_{1/2,\rm Opt} \sim 0.4 R_{25}$), so the stellar and molecular disks track each other very well in their exponential part.

How do the CO and optical sizes relate in our high-z SFGs? For a Gaussian source 50% of the flux is contained within the FWHM, therefore the measured $R_{1/2}$ CO radius for MD94 and BX610 is respectively $R_{1/2,\rm CO} \sim 4.8$ and 4.1 kpc. We can compare directly these numbers with near-IR NICMOS observations of BX610 (Figure 2) that sample the optical disk of that galaxy (Förster Schreiber et al. 2011). Rest-frame 5000 Å observations of BX610 yield an effective radius of $R_{1/2,\rm Opt} \approx 4.6$ kpc, which within the errors is very comparable to the $J = 1-0$ $R_{1/2,\rm CO}$ we obtain. To put disk optical sizes in the $z \sim 0$ context, the typical half-light optical radius of a $M_* \sim 10^{11}$ M$_\odot$ in the SDSS sample analyzed by Shen et al. (2003) is $R_{1/2,\rm Opt} \sim 4$ kpc. The existing HST observations for MD94 (Figure 2) are rest-frame 2500 Å (Peter et al. 2007), which combined with the AGN presence makes it difficult to obtain a reliable disk size (the 4.8 kpc optical radius reported by Tacconi et al. 2013, is from Hα). Surface photometry shows that 80% of the 2500 Å light is in an exponential component with $R_{1/2,\rm Opt} = 0.37 \pm 0.08$ arcseconds (3.1 ± 0.7 kpc) using the Fisher & Drory (2008) methodology. Converting these measurements to an optical size is, however, not straightforward even in local galaxies (which display a range of scalings, Taylor et al. 2005; Muñoz-Mateos et al. 2007), much less in the poorly characterized high-z population.

It is interesting to compare our results to some other resolved measurements of high-z SMGs. Bothwell et al. (2010) analyze resolved observations of intermediate excitation CO $J = 3-2$ and $J = 4-3$ in several such galaxies at $z \sim 1.2$ to $z \sim 2$. Their typical CO 50% emission radii (computed as the harmonic mean of the major and minor axis) are $R_{1/2,\rm CO} \sim 3$ kpc, although the observations span a range of $R_{1/2,\rm CO} \sim 1-5$ kpc. Similar measurements are reported by Tacconi et al. (2008) and Engel et al. (2010), who find typical CO sizes $R_{1/2,\rm CO} \lesssim 4$ kpc. Sharon et al. (2015) find lensing-corrected source sizes of $R_{1/2,\rm CO} \sim 1.7$ kpc in $J = 3-2$ and $R_{1/2,\rm CO} \sim 2.0$ kpc in $J = 1-0$ for the two components of the $z \sim 2.7$ SMG they study. The $R_{1/2,\rm CO} \sim 4.1$ and 4.8 kpc sizes measured here suggest that the CO $J = 1-0$ disks of main sequence galaxies tend to be somewhat more extended than the region producing mid-J CO emission in SMGs at comparable redshift. On the other hand, resolved CO $J = 1-0$ measurements of five $z \sim 2$ SMGs by Ivison et al. (2011) find complex morphologies with radii of $\gtrsim 6$ kpc for four of the objects (the fifth is unresolved) and a median FWHM linewidth of 540 km s^{-1}. These SMG CO $J = 1-0$ sizes and linewidths are larger than those measured for the same objects in the mid-J transitions, and also larger than the disk sizes we measure here.

The similarity between the molecular and optical sizes in main sequence galaxies is also seen in the CO $J = 3-2$ measurements reported by Tacconi et al. (2013), mostly obtained for $z \sim 1$ sources (Fig. 3). These measurements suggest that $z \sim 2.3$ main sequence galaxy disks follow a scaling between optical light and CO $J = 1-0$ similar to that in local disks. The CO is not measurably more extended than the stars, as may occur if a significant amount of pre-enriched newly-arrived material is present in the disk outskirts. Such pre-enriched material is unlikely to arrive through smooth accretion; it seems much more likely that occurs through mergers, and in particular minor mergers given the placement of these galaxies on the main sequence. The fact that the scaling between CO-emitting molecular gas and the stars is similar to that observed in local disks suggests that we are not catching these $z \sim 2$ main-sequence disks at an out-of-equilibrium stage. Rather, we observe them in an equilibrium situation where the established stellar population and the enriched CO-bright molecular gas that fuels the current star formation have similar radial distributions.

3.2. *Molecular Masses and Surface Densities*

The excellent signal-to-noise of the observations for MD94 and BX610 permits, in principle, a precise determination of their CO $J = 1-0$ luminosity. Unfortunately there is a distressing level of inconsistency between the fluxes measured in the C and D configurations, particularly for MD94, with the former being higher than the latter. After detailed inspection of the data and calibrations it is not clear what to attribute these differences to. In particular, the changes in the flux measured for the sources between D and C configurations are not mirrored by changes in the flux of their respective gain calibrators which could suggest systematic problems with the flux calibration (for MD94 the change is in the opposite direction), and are not due to the phase noise as measured on the gain calibrator (which shows RMS$\sim 10-20$ degrees in either configuration). After application of the calibrations we also recover the expected flux for the sec-

ondary calibrator used in D-array, as noted in §2. The flux inconsistency in MD94 is at the $\sim 2\sigma$ level, which suggests that it could be simply due to noise, much higher for the C-array data. The fact that the C-array observations were obtained during a transition period for the instrument may also have had an effect on the accuracy of those fluxes. Because of these considerations we base our discussion on the fluxes from the naturally weighted combination of C+D observations, which gives preferential weighting to the D-array data and has the best signal-to-noise.

To compute the molecular masses we use Eq. 3 in Bolatto et al. (2013), which is applicable to CO $J = 1 - 0$, with a Galactic CO-to-H_2 conversion factor. This conversion relies fundamentaly on two assumptions: 1) the molecular gas is primarily self-gravitating, and 2) the ratio $\sqrt{\rho}/T$ between gas density, ρ, and temperature, T, is roughly similar to that in local galaxy disks (Bolatto et al. 2013, and references therein). We use $\alpha_{\rm CO} = 4.36$ $M_\odot$ (K km s^{-1} pc^2)$^{-1}$ which includes the Helium contribution to the mass as is customary ($\alpha_{\rm CO} = 3.2$ $M_\odot$ (K km s^{-1} pc^2)$^{-1}$ without the Helium contribution). A number of arguments point to an approximately Galactic value of the conversion factor for main sequence high-z galaxies (Tacconi et al. 2010; Daddi et al. 2010a; Genzel et al. 2012), including the similarity between the gas masses inferred from CO and from dust (Genzel et al. 2015). This is supported by detailed numerical modeling of high-z galaxies, which suggests that the average $\alpha_{\rm CO}$ in these systems is not significantly different from $\alpha_{\rm CO}$ in local disks (Bournaud et al. 2014a). We will see in §3.3 that there are indications that the molecular gas temperature is higher in these sources than the average in GMCs in the Galaxy. It is important to remark that this does not automatically translate into a lower-than-Galactic $\alpha_{\rm CO}$. In a self-gravitating cloud what matters is the $\sqrt{\rho}/T$ ratio, not just the temperature, as stated in assumption number two above. Indeed, there are indications that densities (certainly column densities) are much higher in these objects than in Galactic GMCs.

Under these assumptions, the molecular masses inferred from CO $J = 1 - 0$ for MD94 and BX610 are $M_{\rm mol} \approx 1.7 \times 10^{11}$ and 1.1×10^{11} $M_\odot$ respectively. These masses are similar to the stellar masses determined for these galaxies (Tacconi et al. 2013), resulting in molecular gas fractions of $f_{gas} \sim 50\%$. Bolatto et al. (2013) discuss a surface density correction that is applicable if the CO-emitting gas is not self-gravitating but bound to the overall potential of the galaxy as is applicable in a merger and some galaxy centers (c.f., their Eq. 31). For our galaxies, application of this correction would amount to reducing their molecular mass by a factor of ~ 3. This is consistent with what detailed modeling recovers for very turbulent starbursting mergers, but it is likely too large a correction for the galaxies presented here (by contrast modeling of very actively star-forming clumpy main sequence galaxies finds $\alpha_{\rm CO}$ within 20% of the Galactic value Bournaud et al. 2014a).

Given the sizes we measure for the molecular emission, the molecular masses inferred for MD94 and BX610 imply corresponding average deprojected surface densities of $\Sigma_{\rm mol} \sim 900$ $M_\odot$ pc^{-2} ($i \sim 40°$) and 400 $M_\odot$ pc^{-2} ($i \sim 65°$) assuming the disk size is that of the deconvolved major axis and the measured elongation is due to projection effects ($\Sigma_{\rm mol} \sim 1200 - 1100$ $M_\odot$ pc^{-2} in projection). The surface density found for BX610 is approximately the typical $\Sigma_{\rm mol} \sim 400$ $M_\odot$ pc^{-2} inferred by Freundlich et al. (2013) using position-velocity information in four $z \sim 1.2$ galaxies, as well as spatially-resolved measurements in $z \sim 1.5$ galaxies (Tacconi et al. 2010; Genzel et al. 2013). MD94, on the other hand, exhibits higher deprojected disk surface densities than BX610 mostly as a consequence of its smaller inferred inclination, that place it at the upper end of the Freundlich et al. measurements. We note that these "deprojected" estimates are very tentative and, although more physically interesting than projected quantities, also considerably more uncertain because of the poor knowledge of the geometry. In particular, using the Hα-derived inclination of BX610 (see next paragraph) would result in a deprojected $\Sigma_{\rm mol} \sim 900$ $M_\odot$ pc^{-2}.

We can also extract size and velocity information from the data cubes themselves, and obtain dynamical mass estimates. We use GalPak3D, a Bayesian multiparameter Markov Chain Monte Carlo fitter for 3D galaxy data that takes into account the effects of instrumental resolution (Bouché et al. 2015), to fit the robust C+D cubes for MD94 and BX610. The process requires a starting set of assumptions (source center, size, inclination, velocity dispersion, etc), that are then used to produce a 3D model that is compared to the data to compute a reduced χ^2 figure-of-merit which is then minimized. All resulting estimates are extremely tentative given the resolution and signal-to-noise of the data (Figure 4). The reduced χ^2 resulting from the minimization are 1.15 and 1.05 for MD94 and BX610 respectively, showing that the model is a good fit to the data. The minimum, however, is shallow, showing that the models are not unique. BX610 is fit by a (thick) rotating disk with a maximum velocity of $v_{rot} \sim 220$ km s^{-1} and intrinsic dispersion $v_{disp} \sim 40$ km s^{-1}, inclination of $i \sim 50°$, and radius $R_{1/2,\rm CO} \sim 0.4''$. These parameters are comparable to those obtained from the analysis of its Hα kinematics (Cresci et al. 2009, Table 2), although both the rotational velocity and radius are lower (the latter is also lower than the radius we obtain from the integrated intensity map), and the inclination is higher. The resulting dynamical mass computed as $M_{dyn} = 2\,R_{1/2,\rm CO} v_{rot}^2/G$ using the more robust $R_{1/2,\rm CO} = 4.1$ kpc estimate from Table 2 is $M_{dyn} \sim 1.1 \times 10^{11}$ $M_\odot$, lower than found by Cresci et al. (2009) and too low compared to the inferred baryonic mass $M_* + M_{\rm mol} \simeq 2.1 \times 10^{11}$ $M_\odot$. This is, however, entirely attributable to the inclination found in the CO fit. If we instead use the Hα- derived inclination ($i \sim 33°$) we correct v_{rot} to ~ 310 km s^{-1}, resulting in $M_{dyn} \sim 2.0 \times 10^{11}$ $M_\odot$ in excellent agreement with the estimate of the baryonic mass (we do not expect dark matter to make a significant contribution inside $R_{1/2}$). MD94, on the other hand, is fit as a dispersion-dominated system ($v_{disp} \sim 180$ km s^{-1} and $v_{rot} \sim 60$ km s^{-1} with $i \sim 45°$). The corresponding dynamical mass is $M_{dyn} \sim 0.9 \times 10^{11}$ $M_\odot$, too low to accommodate even the stellar mass. Unfortunately there are no Hα kinematics to compare with, and the example of BX610 highlights the uncertainties of the analysis.

An interesting local comparison may be provided by the starbursting region of the nearby galaxy NGC253, which has 50% of its CO emission within an area of 150×50 pc in projected size with a luminosity $L_{CO} \approx 3.3 \times 10^8$ K km s^{-1} pc^2 (Leroy et al. 2014, Table 5). That region of NGC253 has a star formation rate SFR$\sim 2-3$ M$_\odot$ yr^{-1}, while MD94 and BX610 have inferred integrated SFR$\sim$ 271 and 212 M$_\odot$ yr^{-1} respectively (Tacconi et al. 2013). About ~ 100 NGC253-like complexes filling $\sim 2\%$ of the area of these main sequence disks would be compatible with our CO luminosity and surface brightness, while simultaneously fueling the observed star formation activity. This conceptual "picture" of an agglomeration of starburst-like regions also fits the r_{31} excitation as we discuss in the next section. Note, however, that there is no deep physical significance to the inferred beam filling area other than the fact that it reproduces the observed integrated surface brightness.

3.3. *The Excitation of CO*

The Cosmic Microwave Background (CMB) has a temperature of $T_{CMB} \approx 9$ K at $z \approx 2.3$, which sets an effective floor for the physical temperature of the cold molecular gas (see e.g., da Cunha et al. 2013). In terms of the Rayleigh-Jeans brightness temperature (radiation temperature) measured by the interferometer, the CMB presents a background that lowers the contrast. Thus even for optically thick, thermalized emission the observed Rayleigh-Jeans brightness temperature is systematically lower than the excitation temperature, T_{ex}, and vanishes when $T_{ex} = T_{CMB}$ in the rest frame (see Eq. 6 in Bolatto et al. 2013, which is applicable to the rest frame). The fact that we see relatively bright CO $J = 1-0$ and $J = 3-2$ emission already says that $T_{ex} \gg 9$ K.

The effect of the CMB on the ratio of two transitions is small unless the excitation temperature of the emission is very low. The $S_{\rm CO}\Delta v$ integrated flux ratio between the $J = 3-2$ and $J = 1-0$ transitions is 10.6 ± 1.5 for MD94 and 8.3 ± 1 for BX610. Converting to ratios in brightness temperature units requires dividing by the ratio of upper level quantum numbers, J^2, resulting in $r_{31} \approx 1.17 \pm 0.17$ and $r_{31} \approx 0.92 \pm 0.11$ for MD94 and BX610 respectively. These data have much better signal-to-noise in CO $J = 1-0$ than observations used by Aravena et al. (2014) to measure $r_{31} = 0.58^{+0.21}_{-0.13}$ in BX610, and the r_{31} we obtain is at the 1.5σ upper boundary of the previous measurement.

Under the assumption of coextensive emission, these integrated numbers suggest that the T_{ex} of the $J = 1-0$ and $J = 3-2$ transitions are very similar, and both transitions arise from optically thick warm gas (that is, gas with excitation and kinetic temperature significantly higher than the $E_{32}/k \approx 16.6$ K energy necessary to collisionally jump from $J = 2$ to the $J = 3$ level, where k is Boltzmann's constant).

The data strongly suggest that the emission in CO $J = 1-0$ and $J = 3-2$ is coextensive in these objects. The source sizes are very similar in both CO transitions in BX610, where the measured sizes of the CO emission for the $J = 1-0$ and $J = 3-2$ transitions are the same within the uncertainties ($R_{1/2} = 4.1 \pm 1.1$ kpc for $J = 1-0$, $R_{1/2} = 3.2 \pm 0.6$ kpc for $J = 3-2$). Moreover, the spectral shape of the emission is very similar for both transitions in MD94 and BX610, within the uncertainties associated with the noise (Figure 5). The respective linewidths in CO $J = 1-0$(CO $J = 3-2$) from Single Gaussian fitting are 296 ± 66 (430 ± 61) km s^{-1} and 294 ± 49 (266 ± 35) km s^{-1} respectively (the difference in the case of MD94 is driven by the blue side of the spectrum, where the fit to $J = 3-2$ incorporates as line a wider range of velocities resulting in a shift of the centroid). Averaging these results yields a typical $\Delta v(J = 1-0)/\Delta v(J = 3-2) = 0.90 \pm 0.15$ on average for these two sources. This suggests that, within our ability to quantify them with the present data, no dramatic excitation gradients are present, as both transitions sample the same gas kinematics. This is in contrast with what may be the situation in SMGs, where Ivison et al. (2011) find a measurably larger typical linewidth for the CO $J = 1-0$ in comparison to $J = 3-2$, suggesting the colder gas is more extended. Note, however, that this is a subtle $\sim 15\%$ effect in the SMG sample, and so it could go undetected in our data.

These results point to a molecular gas excitation that is high and uniform in MD94 and BX610, up to the $J = 3$ level. Given the widespread molecular emission, the large average gas surface densities, and the inferred SFRs, this should not be surprising. The excitation requirements for the $J = 3-2$ transition are not particularly stringent: $T \gtrsim E_{32}/k \approx 16.6$ K, and an effective critical density $n_{crit} \approx 2 \times 10^4/\tau_{\rm CO\ 3-2} \sim$ few $\times 10^3$ cm^{-3}, making the r_{31} ratio a rather blunt indicator of excitation. By comparison, the average relation for dust temperature along the main sequence predicts $T_{dust} \sim 31$ K for these objects (Genzel et al. 2015, Table 5), which can be taken as a proxy for the gas temperature in dense environments and certainly meets the requirement for excitation to $J = 3$. The measured r_{31} values show that there is not a large reservoir of cold and/or diffuse low excitation molecular gas, bright in CO $J = 1-0$ but not apparent in $J = 3-2$, present in these sources.

In a study using a library of galaxy simulations, Narayanan & Krumholz (2014) make the case for the link between $\Sigma_{\rm SFR}$ and CO line ratios in galaxies. They show that in moderately active star-forming galaxies ($\Sigma_{\rm SFR} \gtrsim 0.2$ M$_\odot$ yr^{-1} kpc^{-2}) the molecular gas has average temperatures larger than the energy of the $J = 3$ level, and given its large typical optical depth it is very easy to excite this transition through collisions and radiative trapping. In particular, they parametrize the expected line ratios as a function of $\Sigma_{\rm SFR}$. Using their Eq. 19 and the $\Sigma_{\rm SFR} \gtrsim 2-3$ M$_\odot$ yr^{-1} kpc^{-2} measured for our galaxies, we would expect $r_{31} \sim 0.9$, very similar to what we measure.

Interestingly, our results are also consistent with the r_{31} measured for CO in the central regions of NGC253 (Bradford et al. 2003). Another point of comparison is provided by the nearby Seyfert NGC1068. There the line ratio averages to $r_{31} \sim 1.2$ in the starburst ring, but with a large range of values correlated with the local star formation activity measured in Paschen α: $r_{31} \sim 0.7-1$ in regions with low SFR, and $r_{31} \sim 2-3$ in regions with high SFR (Garcia-Burillo et al. 2014). The compact circumnuclear disk region, heavily influenced by the AGN, shows $r_{31} \sim 2.7$.

Actively star-forming $z = 0$ galaxies span a range of r_{31}, and although a typical value is $r_{31} \sim 0.66$ there exist several local examples with $r_{31} \geq 0.9$ (Figure 6; Mauersberger et al. 1999; Yao et al. 2003; Papadopoulos et al. 2011). There has been a tendency to attribute the high r_{31} measured in some high-z sources to the presence of a strong AGN (e.g., Riechers et al. 2011). Nonetheless, it is clear now that at least some high-z sources display high r_{31} ratios with no clear AGN activity (Sharon et al. 2013, 2015). That is certainly the case also in the NGC253 starburst, where no strong AGN is detected, and in the starburst ring of NGC1068 where the influence of the AGN is negligible. It is more likely that r_{31} is not so much acting as an indicator of overall density and temperature, but rather showing how well mixed the star formation activity (which provides the bulk of the gas heating) and the molecular reservoir are. Galaxies where part of the molecular reservoir is quiescent (thus cold and/or diffuse) will show lower r_{31}, while galaxies where most of the molecular gas in experiencing star formation will exhibit higher r_{31} ratios.

4. SUMMARY AND CONCLUSIONS

We present and discuss CO $J = 1 - 0$ observations of four main sequence star forming galaxies at $z = 2.2 - 2.3$ that are part of the PHIBSS sample. These observations image and resolve two of these galaxies, MD94 and BX610, with very good signal-to-noise. These galaxies are representative of the luminous and massive end of the main sequence at their redshift. The reader should keep in mind that because they were selected on the basis of their CO $J = 3 - 2$ flux, however, it is unclear whether they are representative of the CO properties of the wider main-sequence population. We use these data to study three aspects of these galaxies:

1. We clearly resolve their molecular disks in CO $J = 1 - 0$, finding half-light CO radii of $R_{1/2,\mathrm{CO}} \approx 4.8$ and 4.1 kpc respectively. We find that the molecular and optical disk of BX610 have half-light sizes that agree within the errors, while MD94 lacks high resolution rest-frame optical observations to compare with. This agrees with the conclusions of Tacconi et al. (2013), derived using CO $J = 3 - 2$ measurements. It is also similar to the observations on local disks where both CO and optical light have very similar length scales (Young & Scoville 1991; Schruba et al. 2011), suggesting that in these $z \sim 2$ main sequence objects we are already observing an equilibrium configuration between the established stellar population and the CO-bright molecular gas fueling star formation. We also observe that the CO $J = 1 - 0$ molecular disk sizes we measure in these main-sequence galaxies are more extended than those typically obtained for mid-J CO emission in SMGs at similar redshifts.

2. We measure molecular masses very similar to the stellar masses of these galaxies, and gas surface densities that are $500 - 900$ $\mathrm{M_\odot}$ $\mathrm{pc^{-2}}$ deprojected, assuming that the CO-to-H_2 conversion factor is similar to the Milky Way (which is supported in general for main sequence galaxies, e.g., Genzel et al. 2015). The CO surface brightness is similar to what would be produced by ~ 100 complexes like that in the center of NGC253 filling $\sim 2\%$ of the area of these disks. This "picture" of a collection of NGC253-like starburst complexes is also consistent with the observed SFR and r_{31} excitation.

3. Comparison of our observations with $J = 3 - 2$ data yields r_{31} ratios that are approximately unity. This, together with the fact that we measure very similar line profiles and disk sizes in both transitions suggests that these sources do not have a large excitation gradient or a significant reservoir of cold or low density molecular gas. Because it is relatively easy to populate the $J = 3$ level of CO in star-forming gas (where star formation supplies the heating needed to raise the gas temperature, e.g., Narayanan & Krumholz 2014), we suggest that r_{31} may act as an indicator of how well-mixed the star formation activity is with the entire molecular reservoir.

We thank Andy Harris for enlightening discussions and comments on earlier versions of this manuscript. We also thank Alice Shapley for providing the HST image of MD94, which includes perfected astrometry. A.D.B. wishes to acknowledge partial support from grants nsf-ast0955836 (CAREER) and nsf-ast1412419, as well as visiting support from the Humboldt Foundation and the Max Planck Institutes for Extraterrestrial Physics and Astronomy.

REFERENCES

Aravena, M., Carilli, C., Daddi, E., et al. 2010, ApJ, 718, 177
Aravena, M., Hodge, J. A., Wagg, J., et al. 2014, MNRAS, 442, 558
Baker, A. J., Tacconi, L. J., Genzel, R., Lehnert, M. D., & Lutz, D. 2004, ApJ, 604, 125
Bolatto, A. D., Wolfire, M., & Leroy, A. K. 2013, ARA&A, 51, 207
Bothwell, M. S., Chapman, S. C., Tacconi, L., et al. 2010, MNRAS, 405, 219
Bouché, N., Carfantan, H., Schroetter, I., Michel-Dansac, L., & Contini, T. 2015, arXiv.org, 6586
Bouché, N., Dekel, A., Genzel, R., et al. 2010, ApJ, 718, 1001
Bournaud, F., Daddi, E., Weiss, A., et al. 2014a, arXiv.org, 8157
Bournaud, F., Perret, V., Renaud, F., et al. 2014b, ApJ, 780, 57
Bradford, C. M., Nikola, T., Stacey, G. J., et al. 2003, ApJ, 586, 891
Brooks, A. M., Governato, F., Quinn, T., Brook, C. B., & Wadsley, J. 2009, ApJ, 694, 396
Carilli, C. L., & Walter, F. 2013, ARA&A, 51, 105
Coppin, K. E. K., Swinbank, A. M., Neri, R., et al. 2007, ApJ, 665, 936
Cresci, G., Hicks, E. K. S., Genzel, R., et al. 2009, ApJ, 697, 115
da Cunha, E., Groves, B., Walter, F., et al. 2013, ApJ, 766, 13
Daddi, E., Dickinson, M., Morrison, G., et al. 2007, ApJ, 670, 156
Daddi, E., Bournaud, F., Walter, F., et al. 2010a, ApJ, 713, 686
Daddi, E., Elbaz, D., —. 2010b, ApJLetters, 714, L118
Daddi, E., Dannerbauer, H., Liu, D., et al. 2014, arXiv.org, 8158
Dannerbauer, H., Daddi, E., Riechers, D. A., et al. 2009, ApJLetters, 698, L178
Davé, R., Finlator, K., & Oppenheimer, B. D. 2011a, MNRAS, 416, 1354
—. 2012, MNRAS, 421, 98
Davé, R., Oppenheimer, B. D., & Finlator, K. 2011b, MNRAS, 415, 11
Dekel, A., Sari, R., & Ceverino, D. 2009a, ApJ, 703, 785

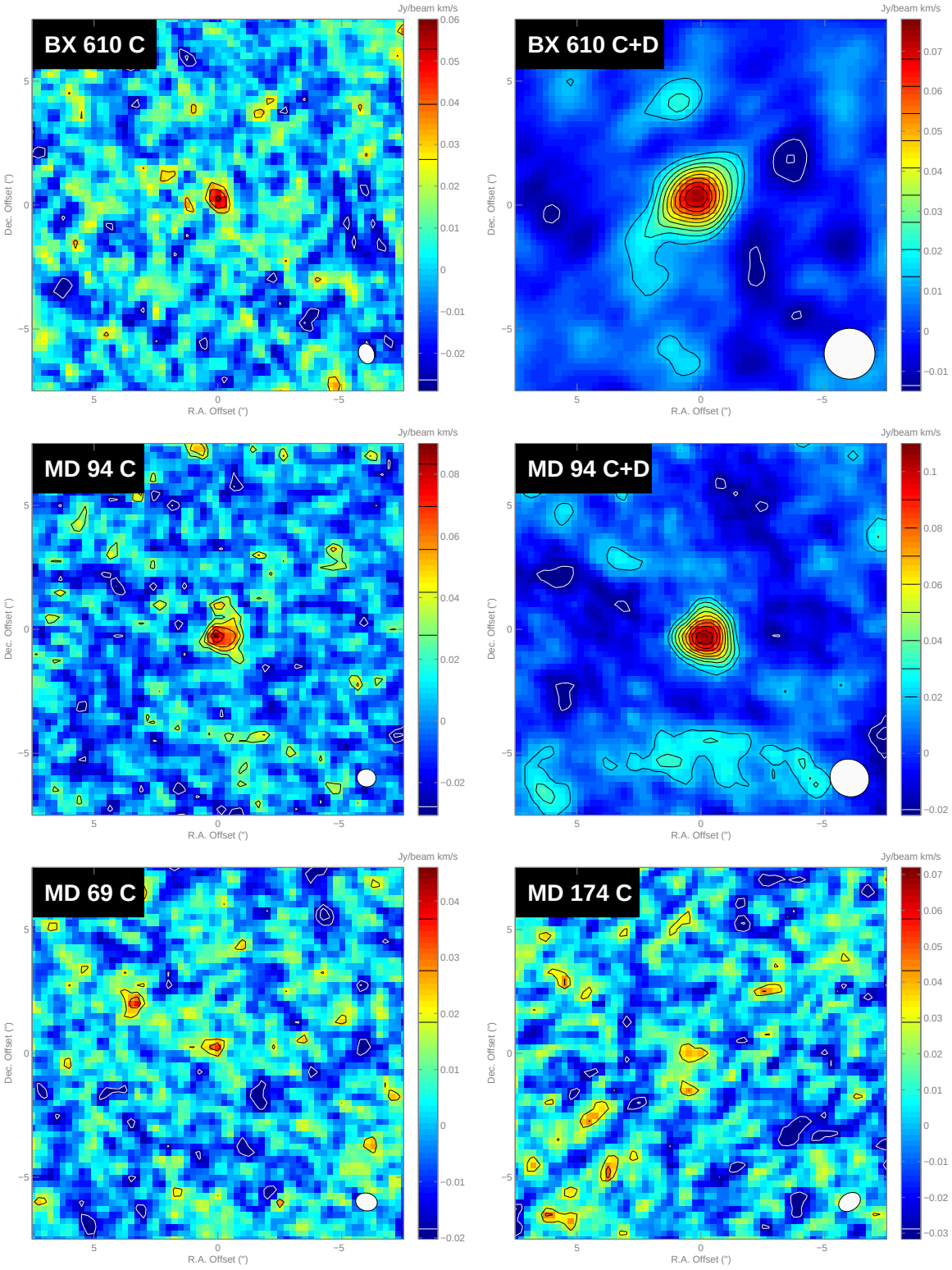

Figure 1. CO $J = 1 - 0$ integrated intensity maps of our $z \sim 2$ main-sequence targets. We show the naturally-weighted C-array observations for our four galaxies, and the naturally weighted C+D combination for MD94 and BX610. The corresponding synthesized beam is illustrated in the bottom-right corner. The contours start at $\pm 2\sigma$ and increase by 1σ, with σ listed in Table 1 (white contours for negative values). The color bar to the right of each panel indicates the intensity scale and the contour values used.

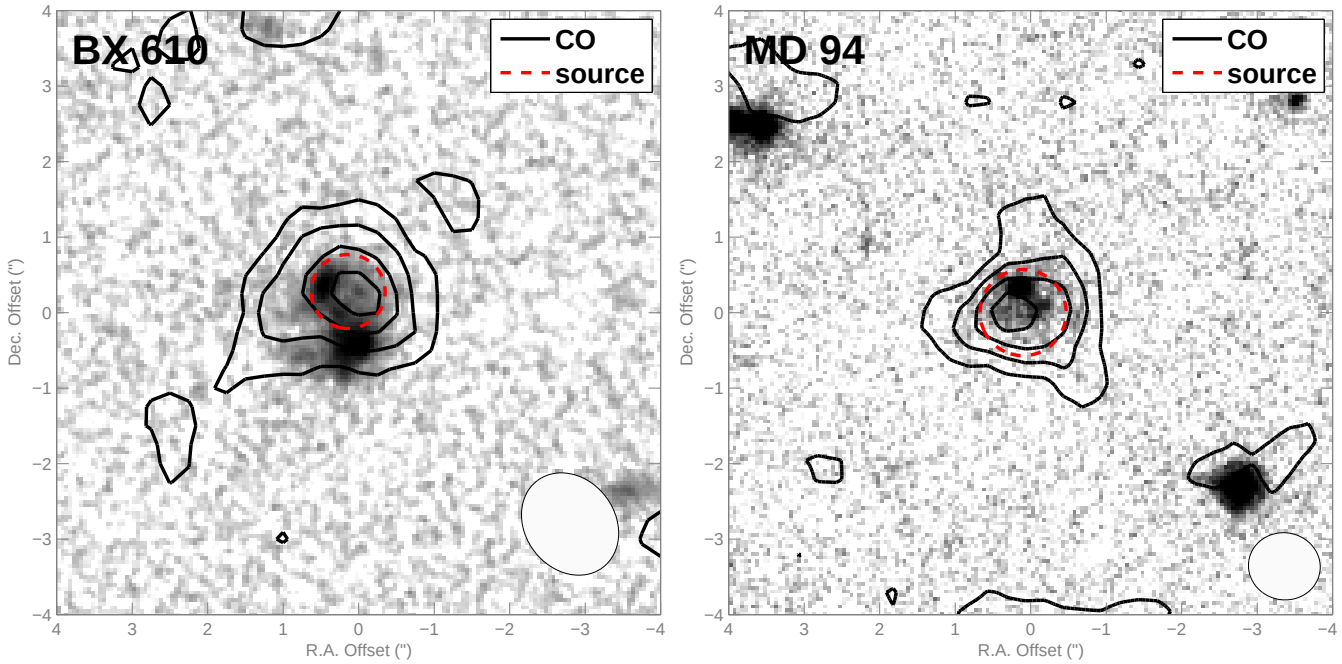

Figure 2. Comparison of CO and HST rest-frame optical or UV data. We show the robust Briggs-weighted combination of C+D array CO $J = 1 - 0$ data in contours (starting at 2σ, in steps of 2σ), overlaid on the HST data. For BX610 the image is HST NICMOS 1.6 μm observations from Förster Schreiber et al. (2011), while for MD94 the image is HST ACS 814 nm from Peter et al. (2007, kindly provided by A. Shapley). The stretch in these images is logarithmic to emphasize the extended emission of the source disks. The corresponding synthesized clean beam is illustrated in the bottom right corner. The dashed circle illustrates the $R_{1/2,\mathrm{CO}}$ for CO $J = 1 - 0$, our best measurement of the intrinsic molecular source size.

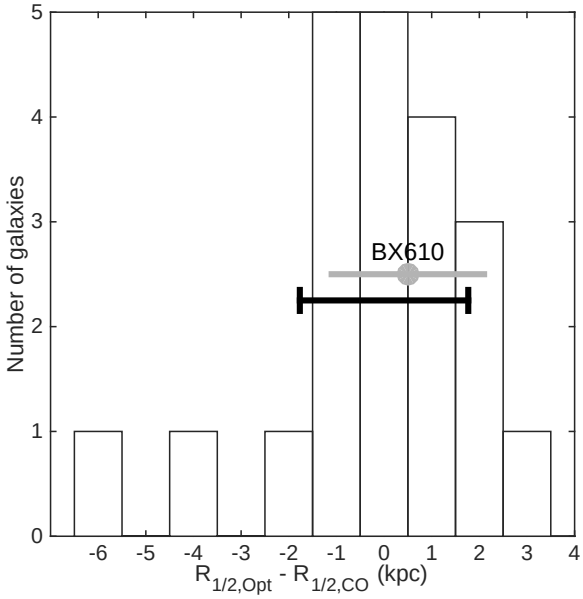

Figure 3. Comparison of optical and CO $J = 3 - 2$ sizes in main-sequence galaxies (mostly $z \sim 1$) reported by Tacconi et al. (2013). The histogram shows the distribution of the difference between $R_{1/2}$ for the optical light, $R_{1/2,\mathrm{Opt}}$, and $R_{1/2}$ for the resolved CO measurements (mostly from $J = 3 - 2$), $R_{1/2,\mathrm{CO}}$. The black horizontal bar illustrates the approximate $\pm 1\sigma$ error in the difference (the typical error in each size determination is ~ 1.3 kpc). The gray bar shows the $J = 1 - 0$ measurement presented here for BX610. The distribution of the difference of optical and molecular sizes shows that in the vast majority of these galaxies the CO and optical light follow each other, with the exception of two galaxies that appear much larger in CO (perhaps undergoing a minor merger).

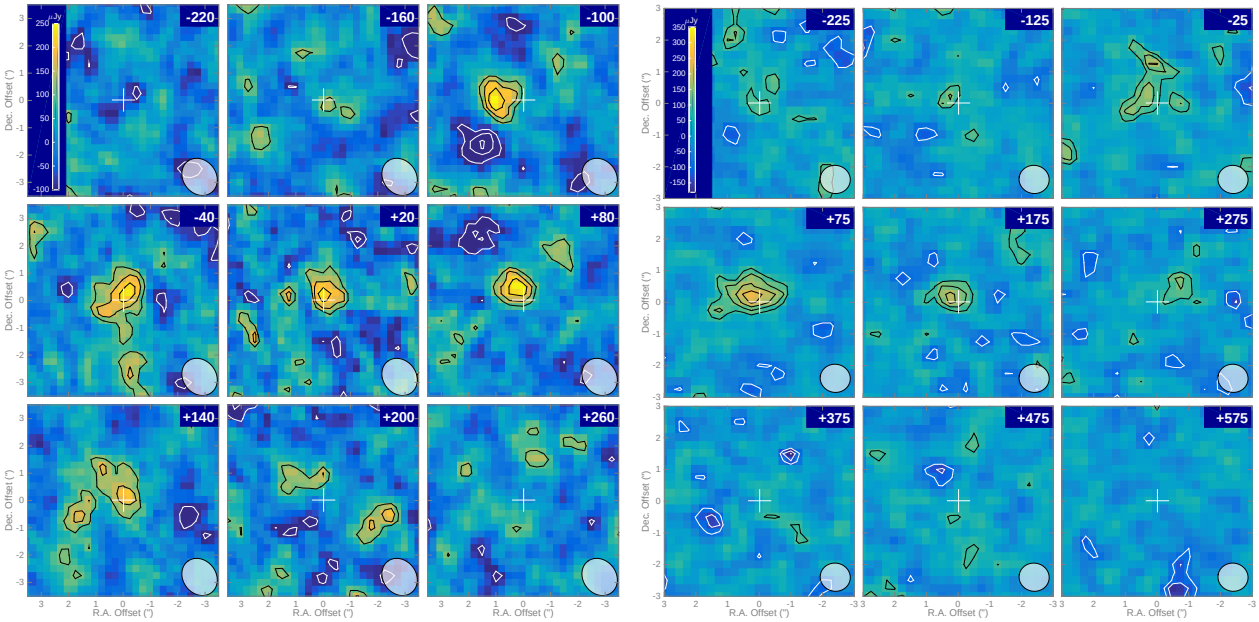

Figure 4. Channel maps showing the $J = 1 - 0$ emission in BX610 (left) and MD94 (right). We show here the robust combination of C+D data. The contours start at 2σ and have increments of 1σ, with positive values in black and negative in white. Note that the velocity interval is 60 km s^{-1} for BX610 and 100 km s^{-1} for MD94. The sythesized beams are shown in the bottom right corner.

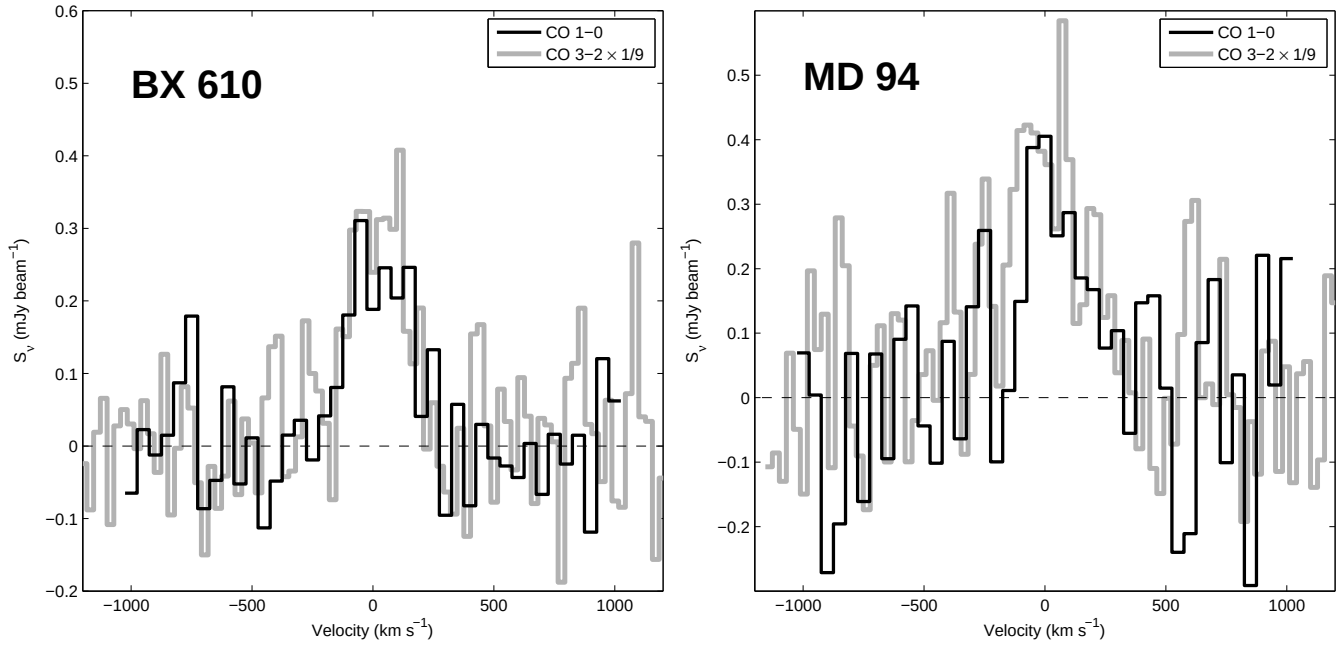

Figure 5. Comparison of spatially integrated spectra of MD94 and BX610 in CO $J = 1 - 0$ and $J = 3 - 2$. The spectral cubes are matched at $2\farcs5$ resolution for BX610 and $5''$ resolution for MD94. The spectral resolution is 50 km s^{-1} for $J = 1 - 0$ and ~ 28 km s^{-1} for $J = 3 - 2$. The panels show the spectra for the center position after spatial resolution-matching. The $J = 3 - 2$ data (in gray) are scaled down by a factor of 9 (i.e., J^2).

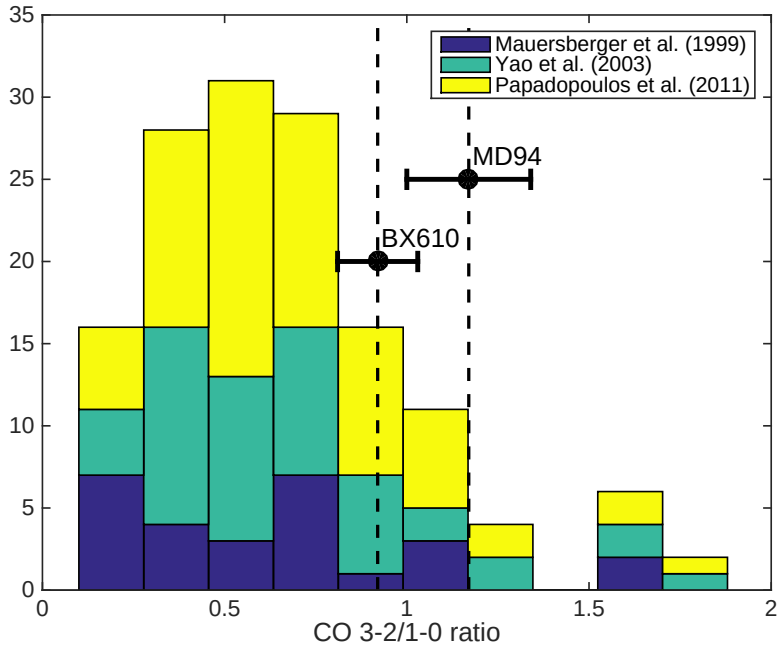

Figure 6. Compilation of r_{31} values in local samples, measured in nearby galaxies (Mauersberger et al. 1999), luminous infrared galaxies (Yao et al. 2003), and ultra-luminous infrared galaxies (Papadopoulos et al. 2011). All samples have very similar mean values of $r_{31} \sim 0.66$. The values measured here for MD94 and BX610 (c.f., Table 2) fall on the high end of the observed range, but are not outliers.

Table 1
Photometry

Dataset	Position (J2000)[d]		σ[e]	$S_{\rm CO}\Delta v$ [d]	$L'_{\rm CO}$	Deconvolved source size[d,f]		
	RA	Dec	(mJy km s^{-1})	(mJy km s^{-1})	(10^{10}K km s^{-1} pc^2)	Major ($''$)	Minor ($''$)	P.A. ($^\circ$)
BX610 C	$23^{\rm h}46^{\rm m}09\overset{\rm s}{.}43$	$12^\circ49'19\overset{''}{.}3$	14[a]	124 ± 35[a]	3.1 ± 0.9	1.0 ± 0.4	0.4 ± 0.2	27 ± 67
BX610 C+D	$23^{\rm h}46^{\rm m}09\overset{\rm s}{.}43$	$12^\circ49'19\overset{''}{.}1$	7[a]	105 ± 10[a]	2.6 ± 0.2	1.6 ± 0.4	0.6 ± 0.4	118 ± 22
BX610 CO 3-2	$23^{\rm h}46^{\rm m}09\overset{\rm s}{.}44$	$12^\circ49'19\overset{''}{.}3$	40[a]	870 ± 63[a]	2.4 ± 0.2	0.8 ± 0.2	0.7 ± 0.2	34 ± 123
MD94 C	$17^{\rm h}00^{\rm m}42\overset{\rm s}{.}00$	$64^\circ11'24\overset{''}{.}3$	14[b]	288 ± 68[b]	7.8 ± 1.5	1.6 ± 0.4	1.0 ± 0.3	6 ± 20
MD94 C+D	$17^{\rm h}00^{\rm m}42\overset{\rm s}{.}01$	$64^\circ11'24\overset{''}{.}2$	10[b]	144 ± 13[b]	3.9 ± 0.4	1.1 ± 0.3	1.0 ± 0.3	114 ± 86
MD94 CO 3-2	$17^{\rm h}00^{\rm m}42\overset{\rm s}{.}13$	$64^\circ11'24\overset{''}{.}6$	170[b]	1520 ± 170[b]	4.6 ± 0.5	...	...	...
MD69 C	$17^{\rm h}00^{\rm m}47\overset{\rm s}{.}67$	$64^\circ09'44\overset{''}{.}3$	10[a]	52 ± 18[a]	1.4 ± 0.5	1.3 ± 0.6	0.2 ± 0.3	81 ± 28
MD174 C	...	...	40[c]	< 120[c]	< 3.3[c]	...	...	...

[a] Integrated over ± 150 km s^{-1}.
[b] Integrated between -250 km s^{-1} and $+500$ km s^{-1} with respect to $z = 2.336$.
[c] Integrated over ± 300 km s^{-1}, the width of the $J = 3 - 2$ emission. Limits are 3σ.
[d] Deconvolved source FWHM diameters from 2D Gaussian fitting using `imfit`.
[e] In a beam, in the integrated intensity map.
[f] For C+D, reported for robust Briggs weighting

Table 2
Galaxy Parameters

Galaxy	Stellar Mass[a] (10^{11} M$_\odot$)	SFR[a] (M$_\odot$ yr^{-1})	Molecular Mass[b] (10^{11} M$_\odot$)	Diameters[c] (kpc)		$R_{1/2,\rm CO}$ (kpc)	$I_{\rm CO}$[d] (K km s^{-1})	$\Sigma_{\rm mol}$[b,e] (M$_\odot$ pc^{-2})	r_{31}
BX610	1.0 ± 0.3	212 ± 74	1.1 ± 0.1	12.2 ± 3.4	4.6 ± 2.5	4.1 ± 1.1	248 ± 135	398 ± 146	0.92 ± 0.11
MD94[f]	1.5 ± 0.5	271 ± 95	1.7 ± 0.2	10.8 ± 1.2	8.3 ± 1.2	4.8 ± 0.4	277 ± 55	928 ± 164	1.17 ± 0.17

[a] From Tacconi et al. (2013).
[b] Assuming a CO-to-H_2 conversion $\alpha_{\rm CO} = 4.36$ M$_\odot$ (K km s^{-1} pc^2)$^{-1}$ which includes the 1.36 Helium correction factor.
[c] Major and minor diameter enclosing 50% of CO emission computed using `imfit`.
[d] $L'_{\rm CO}/(2\pi\, R^2_{1/2})$ resolved integrated intensity, projected on the sky.
[e] Very uncertain deprojected values using size from CO major axis. That has a small effect on MD94, and a much larger effect on BX610. Measured "on the sky" values are $\Sigma_{\rm mol} \sim 1100 - 1200$ M$_\odot$ pc^{-2}.
[f] Contains an AGN (Erb et al. 2006).

Dekel, A., Birnboim, Y., Engel, G., et al. 2009b, Nature, 457, 451
Engel, H., Tacconi, L. J., Davies, R. I., et al. 2010, ApJ, 724, 233
Erb, D. K., Steidel, C. C., Shapley, A. E., et al. 2006, ApJ, 646, 107
Fisher, D. B., & Drory, N. 2008, AJ, 136, 773
Fisher, D. B., Glazebrook, K., Bolatto, A., et al. 2014, ApJLetters, 790, L30
Fixsen, D. J., Bennett, C. L., & Mather, J. C. 1999, ApJ, 526, 207
Forbes, J. C., Krumholz, M. R., Burkert, A., & Dekel, A. 2014, MNRAS, 438, 1552
Förster Schreiber, N. M., Shapley, A. E., Erb, D. K., et al. 2011, ApJ, 731, 65
Förster Schreiber, N. M., Genzel, R., Newman, S. F., et al. 2014, ApJ, 787, 38
Freundlich, J., Combes, F., Tacconi, L. J., et al. 2013, A&A, 553, A130
Garcia-Burillo, S., Combes, F., Usero, A., et al. 2014, A&A, 567, A125
Genzel, R., Tacconi, L. J., Combes, F., et al. 2012, ApJ, 746, 69
Genzel, R., Tacconi, L. J., Kurk, J., et al. 2013, ApJ, 773, 68
Genzel, R., Förster Schreiber, N. M., Rosario, D., et al. 2014, ApJ, 796, 7
Genzel, R., Tacconi, L. J., Lutz, D., et al. 2015, ApJ, 800, 20
Green, A. W., Glazebrook, K., McGregor, P. J., et al. 2014, MNRAS, 437, 1070
Greve, T. R., Leonidaki, I., Xilouris, E. M., et al. 2014, ApJ, 794, 142
Harris, A. I., Baker, A. J., Zonak, S. G., et al. 2010, ApJ, 723, 1139
Ivison, R. J., Papadopoulos, P. P., Smail, I., et al. 2011, MNRAS, 412, 1913
Ivison, R. J., Swinbank, A. M., Smail, I., et al. 2013, ApJ, 772, 137
Kereš, D., Katz, N., Weinberg, D. H., & Davé, R. 2005, MNRAS, 363, 2
Komatsu, E., Bennett, C. L., Barnes, C., et al. 2014, Progress of Theoretical and Experimental Physics, 2014, 06B102
Leroy, A. K., Bolatto, A. D., Ostriker, E. C., et al. 2014, arXiv.org, 2836
Lilly, S. J., Carollo, C. M., Pipino, A., Renzini, A., & Peng, Y. 2013, ApJ, 772, 119
Mauersberger, R., Henkel, C., Walsh, W., & Schulz, A. 1999, A&A, 341, 256
Muñoz-Mateos, J. C., Gil de Paz, A., Boissier, S., et al. 2007, ApJ, 658, 1006
Narayanan, D., & Krumholz, M. R. 2014, MNRAS, 442, 1411
Newman, S. F., Buschkamp, P., Genzel, R., et al. 2014, ApJ, 781, 21
Noeske, K. G., Weiner, B. J., Faber, S. M., et al. 2007, ApJ, 660, L43
Oppenheimer, B. D., Davé, R., Kereš, D., et al. 2010, MNRAS, 406, 2325
Papadopoulos, P. P., van der Werf, P., Xilouris, E., Isaak, K. G., & Gao, Y. 2012, ApJ, 751, 10
Papadopoulos, P. P., van der Werf, P., Xilouris, E. M., et al. 2011, arXiv.org, 4176
Perley, R. A., & Butler, B. J. 2013, ApJS, 204, 19
Peter, A. H. G., Shapley, A. E., Law, D. R., et al. 2007, ApJ, 668, 23
Regan, M. W., Thornley, M. D., Helfer, T. T., et al. 2001, ApJ, 561, 218
Riechers, D. A., Carilli, C. L., Walter, F., & Momjian, E. 2010, ApJLetters, 724, L153
Riechers, D. A., Carilli, C. L., Maddalena, R. J., et al. 2011, ApJLetters, 739, L32
Rodighiero, G., Cimatti, A., Gruppioni, C., et al. 2010, A&A, 518, L25
Schruba, A., Leroy, A. K., Walter, F., et al. 2011, AJ, 142, 37
Sharon, C. E., Baker, A. J., Harris, A. I., et al. 2015, ApJ, 798, 133
Sharon, C. E., Baker, A. J., Harris, A. I., & Thomson, A. P. 2013, ApJ, 765, 6
Shen, S., Mo, H. J., White, S. D. M., et al. 2003, Monthly Notice of the Royal Astronomical Society, 343, 978
Tacconi, L. J., Genzel, R., Smail, I., et al. 2008, ApJ, 680, 246
Tacconi, L. J., Genzel, R., Neri, R., et al. 2010, Nature, 463, 781
Tacconi, L. J., Neri, R., Genzel, R., et al. 2013, ApJ, 768, 74
Taylor, V. A., Jansen, R. A., Windhorst, R. A., Odewahn, S. C., & Hibbard, J. E. 2005, ApJ, 630, 784
Weiss, A., Downes, D., Walter, F., & Henkel, C. 2007, From Z-Machines to ALMA: (Sub)Millimeter Spectroscopy of Galaxies ASP Conference Series, 375, 25
Whitaker, K. E., van Dokkum, P. G., Brammer, G., & Franx, M. 2012, ApJLetters, 754, L29
Yao, L., Seaquist, E. R., Kuno, N., & Dunne, L. 2003, ApJ, 588, 771
Young, J. S., & Scoville, N. Z. 1991, ARA&A, 29, 581
Young, J. S., Xie, S., Tacconi, L., et al. 1995, ApJSupplement Series, 98, 219